Modified Hollow Glass Microspheres/Reduced Graphene Oxide Composite Aerogels with Low Thermal Conductivity for Highly Efficient Solar Steam Generation

Shuo Wang, Ye Niu, Chengjun Wang, Fei Wang, Zhaoqi Zhu, Hanxue Sun, Weidong Liang, and An Li*

Cite This: *ACS Appl. Mater. Interfaces* 2021, 13, 42803−42812

Read Online

ACCESS | Metrics & More | Article Recommendations | SI Supporting Information

ABSTRACT: Solar steam generation (SSG) as a pollution-free and sustainable way for desalination or wastewater treatment has attracted great attention in recent years. Herein, we report the fabrication of novel aerogels GAHAS and GAHAF composed of 3-aminopropyltriethoxysilane (KH550)-modified hollow glass microspheres (HGM) and reduced graphene oxide (RGO) by a sol−gel method for highly efficient SSG. The RGO can well wrap on modified HGM and form an interpenetrated porous structure with an excellent mechanical property. In addition, benefiting from the hollow structure of HGM, GAHAS obtained by supercritical CO_2 drying well maintains the original structure of the hydrogel and shows low thermal conductivity (0.0823 W m^{-1} K^{-1}) in the wet state and self-floating ability. Combined with its superhydrophilic wettability and high light absorption (ca. 93%), the as-prepared GAHAS shows an outstanding photothermal conversion efficiency of 89.13% under 1 sun (1 kW m^{-2}) illumination and excellent stability. Moreover, from the simulated seawater outdoor solar desalination experiment, it was found that the concentrations of the four primary ions K^+, Ca^{2+}, Na^+, and Mg^{2+} in purified water are 1.65, 0.09, 1.42, and 0.32 mg L^{-1}, respectively, and fully meet drinking water standards. Thus, our GAHAS aerogel shows great potential for practical application in SSG. This work enriches the photothermal materials and may provide a new idea for design and creation of HGM-based photothermal materials with low thermal conductivity, tunable porosity, high mechanical strength, self-floating ability, and high solar energy conversion efficiency for SSG.

KEYWORDS: solar steam generation, aerogels, hollow glass microspheres, reduced graphene oxide, desalination
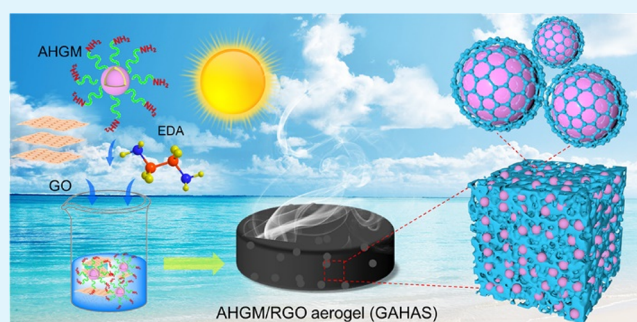
1. INTRODUCTION

With the increase of the world's population, the improvement of living standards, and the rapid development of industries, freshwater scarcity has become a serious global problem.[1,2] Although many technologies, such as multistage flash,[3] multi-effect distillation[4] and reverse osmosis,[5] etc., have been employed for clean water production, they mainly rely on the consumption of nonrenewable energy sources such as fossil fuels and electricity, which aggravated the energy crisis accompanied by serious environmental pollution. As a renewable and clean energy, solar energy is applied in many fields.[6−9] Most recently, as one of the most promising water cleaning techniques, solar steam generation (SSG) has attracted significant attention not only because it uses inexhaustible and clean solar energy but also because of its unique "interfacial vaporization" manner to produce freshwater using a photothermal material with high energy conversion efficiency instead of the traditional water evaporation by heating the bulk water with a large heat loss.[10−13]

In order to achieve excellent evaporation performance and realize the practical application of SSG for water purification or desalination, as the key component of an SSG system,

photothermal materials should have the properties including excellent absorption of sunlight, a porous and hydrophilic structure for fast water transportation, good thermal insulation to minimize heat loss, etc.[14−16] Following these complementary design principles, so far, a wide variety of photothermal materials have been developed, including metallic nanoparticles,[17] polymer-based materials,[18,19] biomass-based materials,[20−22] and hydrogels.[23−25] Among these different types of developed photothermal materials, aerogels have a coherent open three-dimensional porous structure with a high specific surface area, low thermal conductivity, and low density. They are the best choice for photothermal materials, and so far, many aerogel-based photothermal materials have been created.[26,27] For instance, the conjugated microporous polymer
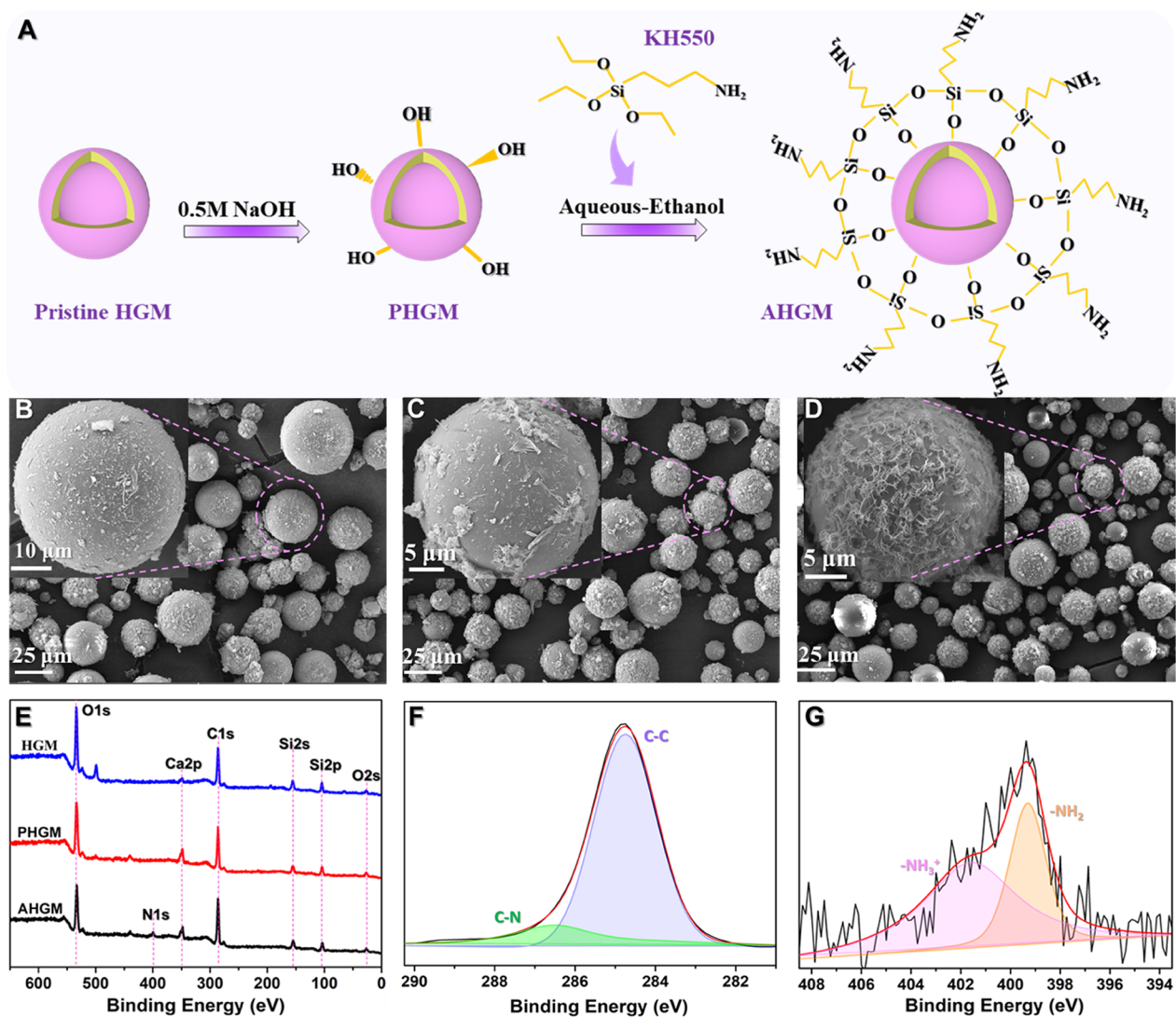
Figure 1. (A) Schematic illustration of the preparation process of AHGM. (B−D) SEM images of (B) HGM, (C) PHGM, and (D) AHGM. (E) XPS spectra of HGM, PHGM, and AHGM. (F) C 1s XPS spectrum of AHGM. (G) N 1s XPS spectrum of AHGM.

nanotube aerogels have been reported by our group;[28] they can achieve high energy conversion efficiency (86.8%) under 1 sun illumination. Wang *et al.*[29] prepared nanofibrous aerogel with vertically aligned microchannels and the energy efficiency of the aerogel is up to 90.3% under 1 sun illumination. In particular, graphene-based photothermal materials have attracted great interest due to their excellent optical absorption and high energy conversion efficiency.[30] Aerogels take advantage of the pore structure and surface chemical properties that can be tailored. However, many challenges still remain, such as high production cost that limits their large-scale application, in most cases, the structure of aerogels easily collapses, especially in water, poor stability of their mechanical property, etc. Therefore, it is of special significance to develop photothermal materials that can meet the mentioned criteria.

Hollow glass microspheres (HGM) are a kind of hollow micrometer-sized inorganic functional powder with low thermal conductivity, low production cost, good dispersion, high strength, low density, excellent mobility, and chemical stability, which have been widely used in many fields, e.g., aerospace,[31] coatings,[32] and thermal insulation materials.[33,34] In particular, the excellent properties allow HGM to self-float

on water, show good thermal insulation, and be used as a reinforcing agent of composite materials, which make HGM quite attractive in the field of photothermal materials. However, to our knowledge, HGM have not been applied in this field. In addition, due to the fact that HGM are mainly composed of silicon dioxide and with low effective functional groups, the surface modification of HGM by a silane coupling agent can make them compatible with organic matter. In this work, for the first time, we propose a new approach for the fabrication of 3-aminopropyltriethoxysilane (KH550)-modified HGM/reduced graphene oxide (RGO) composite aerogels as photothermal materials for efficient SSG. Obviously, such aerogels integrate the merits of both HGM and RGO to construct a mechanically robust structure, which can float on water for a long time without breaking or deforming. Moreover, benefiting from strong light absorption, hydrophilic surface wettability, and excellent thermal insulation of prepared GAHAS, they show high energy conversion efficiency (89.13%) under 1 sun illumination, and the purified water can fully meet the drinking water standard. The findings of this work enrich the photothermal materials and provide a new idea for future design of photothermal materials.
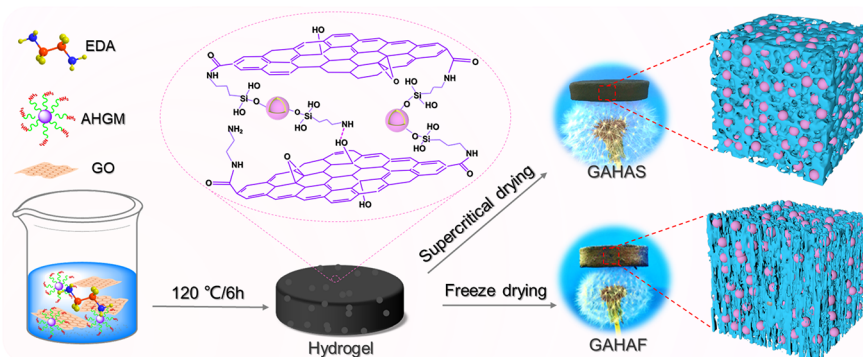
Figure 2. Schematic illustration of the preparation process and structures of GAHAF and GAHAS.

2. EXPERIMENTAL SECTION

2.1. Materials. 3-Aminopropyltriethoxysilane (KH550, 99%) was purchased from Shanghai Macklin Biochemical Co., Ltd. Hollow glass microspheres (iM16K) were provided by 3M Co., Ltd., USA. Graphite powder was purchased from BASF Chemical Co., Ltd., Tianjin. The other reagents with analytical grade were provided by commercial sources.

2.2. Surface Modification of HGM. Pristine HGM particles (20 g) were added in 600 mL of 0.5 M NaOH solution in a beaker and stirred for 1.5 h in a water bath at 80 °C. After the suspension was cooled, it was filtered and washed with distilled water until the filtrate was neutral. Then, the solid particles were dried at 60 °C for 24 h to obtain pretreated hollow glass microspheres (PHGM). After that, 10 g of KH550 was added in a mixed solution consisting of 5 mL of ammonium hydroxide, 15 mL of distilled water, and 200 mL of absolute ethanol in the three-neck flask with a condenser tube. After stirring for 30 min at room temperature, 10 g of PHGM were added and stirred in the water bath at 45 °C for 2 h. The suspension was then filtered and washed with ethanol, subsequently, and the solid particles were dried to obtain KH550-grafted HGM (AHGM).

2.3. Preparation of GAHAF and GAHAS. GO suspension was prepared according to a modified Hummers method reported in the literature.[35] To fabricate aerogels, separately, 10 mL of GO suspension (5 mg/mL), 40 μL of ethylenediamine (EDA), and 0.2 g of AHGM were added into the Teflon lining of the autoclave, followed by magnetic stirring for 1 h. Then, the Teflon lining was transferred into an autoclave and reacted at 120 °C for 6 h. After the temperature gradually fell to room temperature, the hydrogel was obtained. Next, the hydrogel is dried by two drying methods. The first method is that the hydrogel was dialyzed in ethanol aqueous solution (10%) for 12 h, and then it was frozen in the refrigerator for 12 h, subsequently; after freeze drying for 36 h, the aerogel was prepared and marked as GAHAF. The second method is that the hydrogel was dialyzed in absolute ethanol for 12 h, and then it was dried by supercritical CO_2 at 40 °C and 8.5 MPa for 3 h; the aerogel was obtained and marked as GAHAS.

3. RESULTS AND DISCUSSION

3.1. Fabrication and Characterization of AHGM. Figure 1A shows the schematic illustration of the preparation process for AHGM. The pristine HGM were treated in NaOH solution to remove impurities and improve the hydroxyl content on the surface of the particles (PHGM). KH550 has two functional groups, namely, ethoxy group and amino group; the ethoxy group can be easily hydrolyzed to form silanol groups (−SiO−H) in ethanol aqueous solution under an alkaline condition. Then, the silanol groups on the hydrolytic product of KH550 could be absorbed into the surface of PHGM and condense with the hydroxyl group on PHGM to form ether bonds as well as between the silanol groups on the hydrolytic product. The AHGM were obtained with an amino

group on the other side of grafted KH550, which is easy to graft with organic matter.

For the pristine HGM of iM16K, their detailed physical properties are shown in Table S3 in the Supporting Information, and they have a true density of 0.46 g cm^{-3} and a diameter (50th %) of 20 μm, provided by the 3M Co., Ltd., USA. Scanning electron microscopy (SEM) analysis was used to investigate the morphologies of the HGM, PHGM, and AHGM, and the results are shown in Figure 1B,D. It can be found that some small pieces attached on the surface of pristine HGM and the surface are relatively smooth. Meanwhile, the surface of PHGM is rough after NaOH corrosion. This is due to the silicates produced by the reaction of the HGM with NaOH, which were covered on the surface of the particles. Compared with PHGM, the surface of AHGM was wrapped with KH550; no silicates and debris were observed.

In order to further demonstrate that KH550 was successfully grafted onto PHGM, X-ray photoelectron spectroscopy (XPS) spectra of HGM, PHGM, and AHGM were measured, and the results are shown in Figure 1E−G. As shown in Figure 1E, both HGM and PHGM contain four elements, including O, Si, C, and Ca. Compared with HGM and PHGM, AHGM present the additional N 1s peak that can be assigned to the N element in KH550 grafted on AHGM. The C 1s spectrum (Figure 1F) of AHGM contains two peaks of C−C and C−N at 284.3 and 286.5 eV, respectively, and the C−N peak was introduced by KH550.[36] As shown in Figure 1G, the N 1s spectrum of AHGM can be deconvoluted into two peaks, and the peak at 401.6 eV can be assigned to protonated ammonium nitrogen (NH_3^+), while the peak at 399.3 eV belongs to neutral amine (−NH_2).[37] The results indicated that AHGM with terminated amine and KH550 had been grafted successfully.

3.2. Fabrication and Characterization of the Aerogels. The fabrication process of GAHAF and GAHAS is illustrated in Figure 2. Ethylenediamine (EDA) as a reducing agent and AHGM as the thermal insulation reinforced material were first mixed with graphene oxide (GO) aqueous solution. After the hydrothermal reaction in the Teflon-sealed autoclave, the GO sheets gradually self-assembled into hydrogels and AHGM were wrapped. Then, the hydrogels were dialyzed with ethanol aqueous solution or absolute ethanol to remove residues followed by freeze drying and supercritical CO_2 drying, respectively. In this hydrothermal reaction process, the hydrothermal reduction temperature and time, the concentration of GO, and the reducing agent are the key parameters that affect the volume shrinkage and structure cracking of hydrogels. As shown in Figure S2, ammonium hydroxide and potassium hydroxide acted as reductants of the
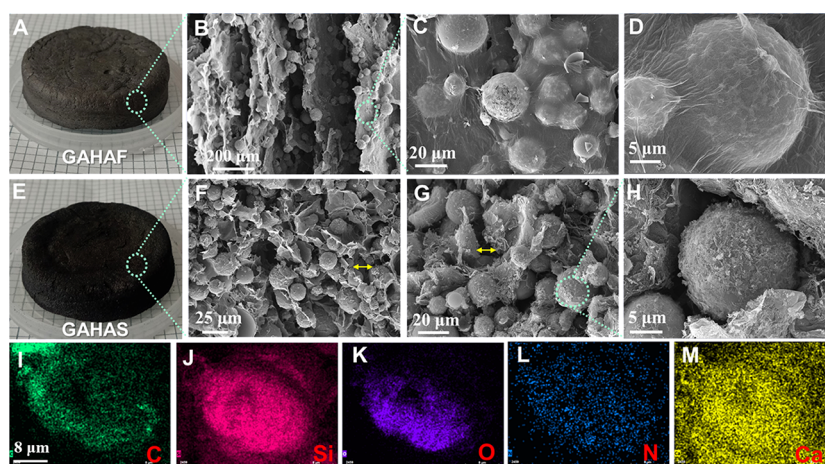
Figure 3. (A) Camera photo of GAHAF. (B−D) SEM images of GAHAF. (E) Camera photo of GAHAS. (F−H) SEM images of GAHAS. (I−M) Elemental maps of GAHAS.
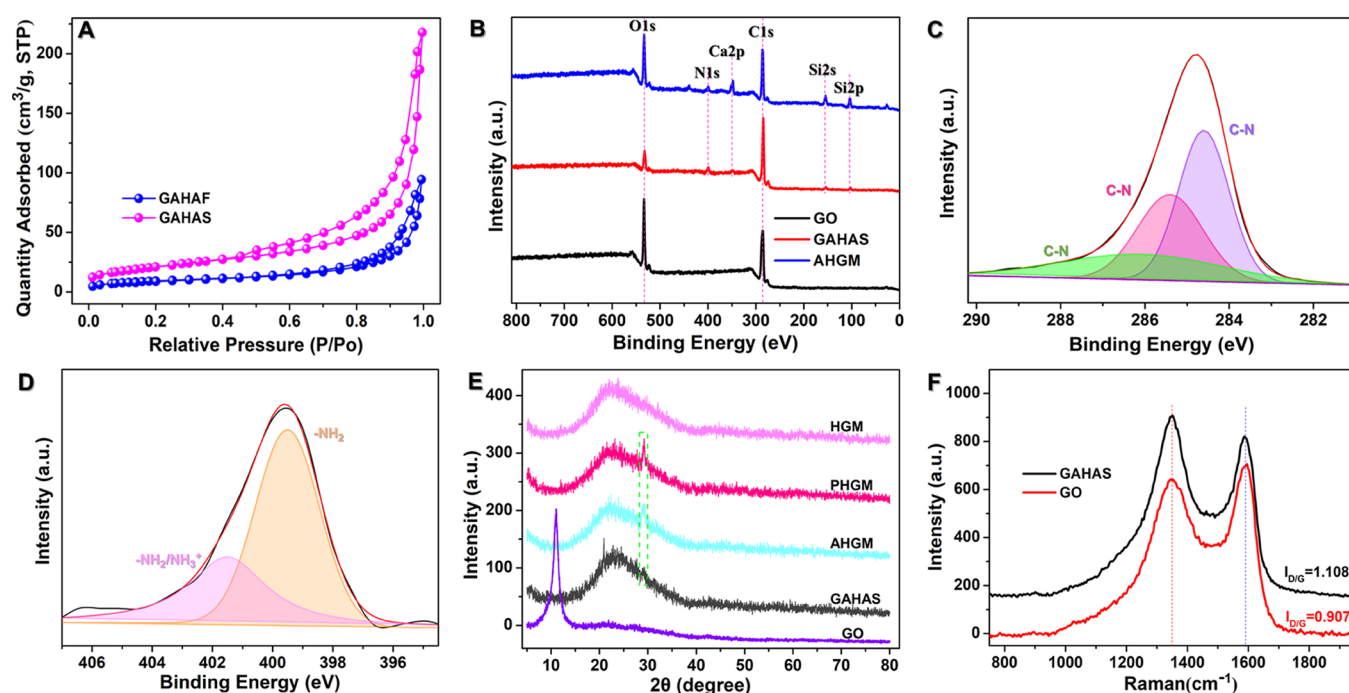

Figure 4. (A) N_2 adsorption/desorption isotherms of GAHAS and GAHAF. (B) XPS spectra of GO, GAHAS, and AHGM. (C) C 1s XPS spectra of GAHAS. (D) N 1s XPS spectra of GAHAS. (E) XRD patterns of GO, HGM, AHGM, PHGM, and GAHAS. (F) Raman spectra of GO and GAHAS.

hydrothermal reaction, and without a reductant, the volume shrinkage of hydrogels were obviously greater compared to when EDA is used as a reductant, while when L-ascorbic acid (L-AA) was used as a reductant, although the volume shrinkage is small, the middle of the hydrogels bulge and is very fragile. In addition, as shown in Figures S3 and S4, the optimal hydrothermal reduction temperature and time are 120 °C and 6 h, respectively. The effect of the concentration of GO was also explored (Figure S5); the volume shrinkage of hydrogels decreased with the increase of GO concentration from 3 to 7 mg mL^{-1}. However, high GO concentration is not conducive to the dispersion of AHGM; the optimal GO concentration was determined as 5 mg mL^{-1}.

The photographs and SEM images of the aerogels are shown in Figure 3A−H. From the digital photographs, GAHAF (Figure 3A) shines with a metal luster, and the color of

GAHAS (Figure 3E) is darker than that of GAHAF. This is mainly related to the temperature of the drying process. As shown in Figure 3B, the morphology of GAHAF is uniform in the large scale and exhibits directional interconnected channels. The pore sizes of the aligned channels ranges from tens to hundreds of micrometers. This is mainly due to the directional growth of ice crystals in the process of freeze casting, which extrudes RGO sheets and AHGM into layered sheets. Figure 3C shows an enlarged view of a single-layered sheet and Figure 3D further shows the morphology of AHGM in the layered sheet. It can be seen clearly that AHGM were distributed uniformly in RGO sheets and were well wrapped by the RGO sheets, which is attributed to the formation of chemical or hydrogen bonds between the amino groups on the surface of AHGM and the oxygen-containing groups on the surface of GO. The SEM images of GAHAS are shown in
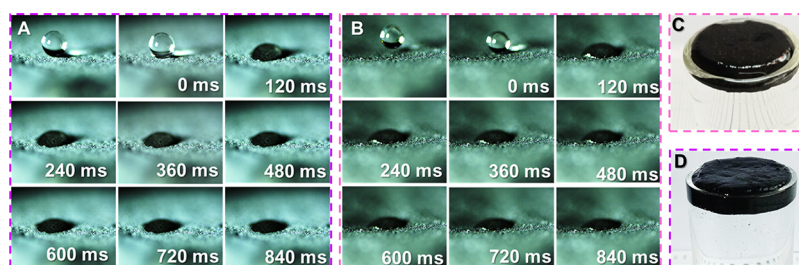
Figure 5. (A) Camera photos of the droplet impregnation process on the surface of GAHAS. (B) Camera photos of the droplet impregnation process on the surface of GAHAF. (C) Camera photo of GAHAF floating on the water surface. (D) Camera photo of GAHAS floating on the water surface.
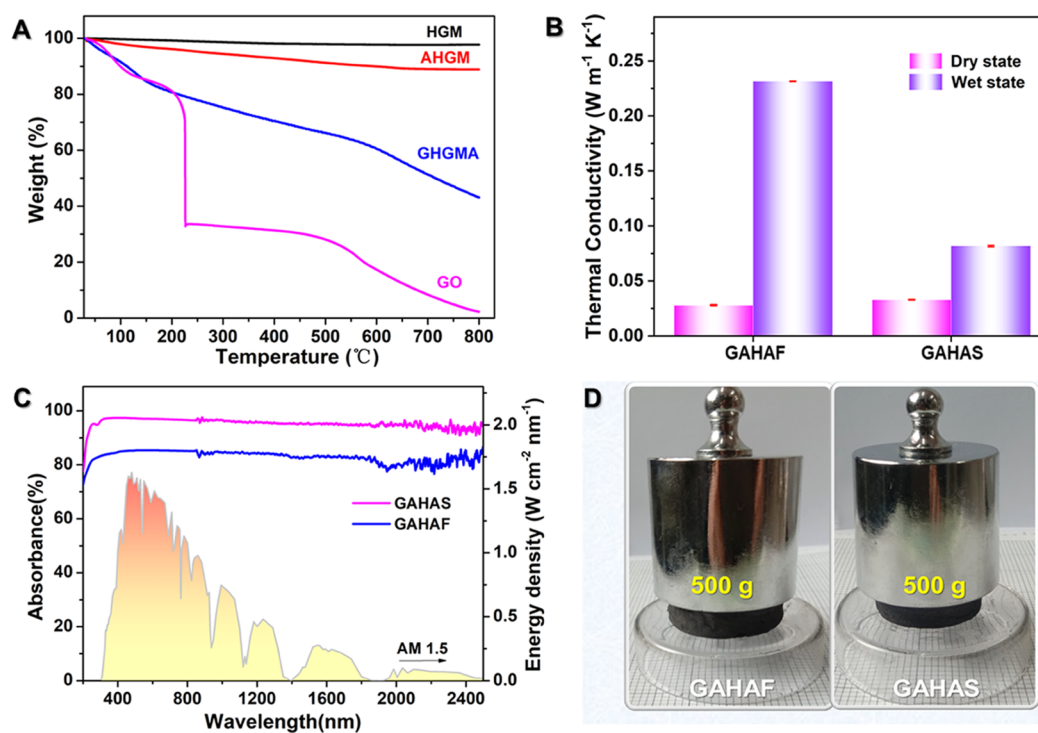

Figure 6. (A) TGA curves of the samples. (B) Thermal conductivity of GAHAF and GAHAS in dry state and wet state. (C) Optical absorption spectra of GAHAF and GAHAS. (D) Camera photos of GAHAF and GAHAS under 500 g weight.

Figure 3HF−. Compared with GAHAF, no directional channels are observed in GAHAS, the RGO sheets in GAHAS are smaller and the small pieces of RGO are wrapped on the surface of the AHGM (Figure 3H). The micrometer-sized pore size of GAHAS ranges from a few micrometers to tens of micrometers. The morphology of GAHAS is mainly attributed to the fact that supercritical CO_2 dried aerogel well maintained the original structure of the hydrogel. In addition, energy-dispersive spectroscopy (EDS) was used to measure the elemental distribution of GAHAS, as shown in Figure 3I−M; the elements of C, Si, O, N and Ca existed on the surface of GAHAS. The elements Si and Ca come from HGM. The N element comes from KH550 grafted on the surface of AHGM and residual EDA.

Except for the micrometer-sized pores in aerogels observed by SEM, the nanosize pore properties of the aerogels were characterized by N_2 adsorption/desorption measurements. As shown in Figure 4A, the N_2 adsorption isotherms of GAHAF and GAHAS belong to type IV according to the IUPAC classification.[38] The adsorptions of GAHAS and GAHAF increase in the P/P_0 range of 0.4−0.9, which indicates that

both samples mainly contain mesopores and macropores. The pore size distribution of the aerogels is shown in Figure S6A,B (GAHAF and GAHAS, respectively), the average pore size was calculated using the Barrett−Joyner−Hallender (BJH) method, and the results are 20.72 nm for GAHAF and 18.12 nm for GAHAS. The BET surface areas of GAHAF and GAHAS are 33.69 and 75.95 m^2 g^{-1}, respectively. The pore volumes of GAHAF and GAHAS are 0.12 and 0.29 cm^3 g^{-1}, respectively. The results show that the nanosize pores of GAHAS are more abundant than those of GAHAF.

The surface chemical composition and functional groups of GO and GAHAS were identified by XPS; as shown in Figure 4B, both GO and GAHAS contain C and O elements, and the peak intensity of the O element in GAHAS is significantly lower than that in GO. The C 1s spectrum of GAHAS (Figure 4C) can be deconvoluted into three subpeaks that correspond to C−C (284.6 eV), C−O (285.4 eV), and C−N (286.1 eV). The N 1s spectrum (Figure 4D) can be divided into −NH$_2$ (399.5 eV) and −NH$_2$/NH^{3+} (401.5 eV), which revealed the functional group −NH$_2$ in EDA and AHGM.[39,40]
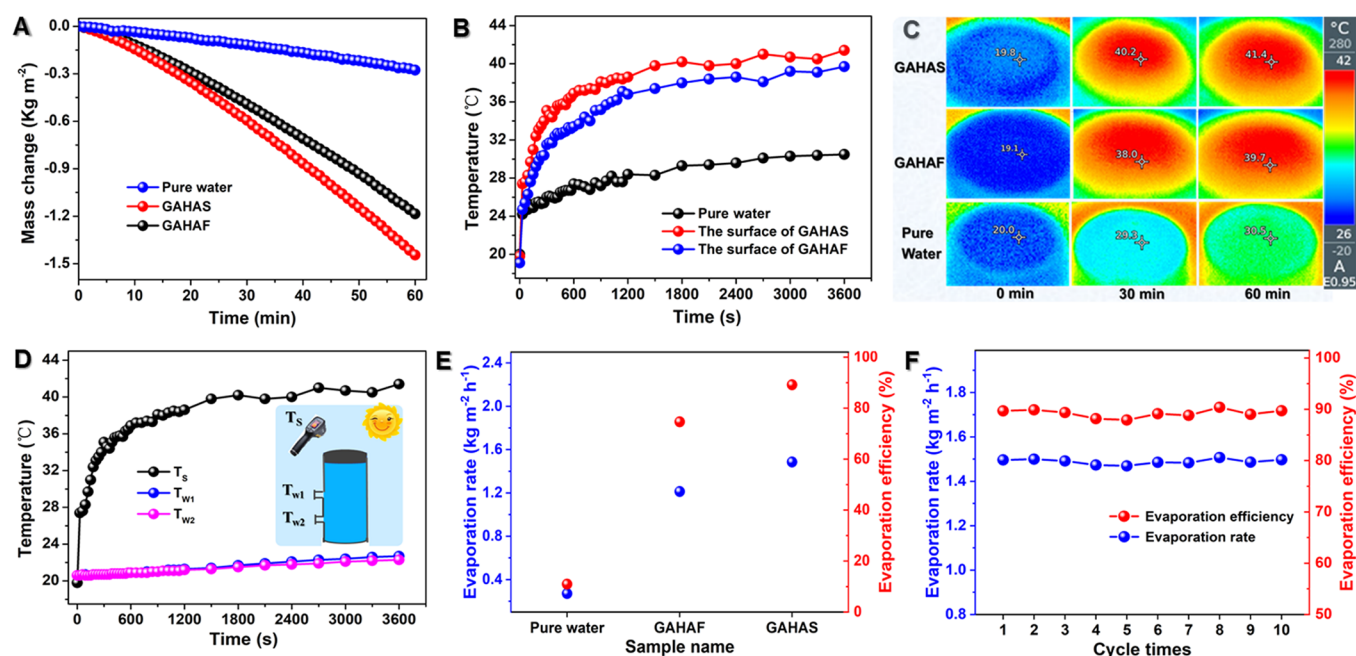
Figure 7. (A) Time-dependent mass changes of pure water, GAHAF, and GAHAS under 1 sun illumination. (B) Surface temperature change curves of pure water, GAHAF, and GAHAS under 1 sun illumination. (C) Infrared images of GAHAS, GAHAF, and pure water with time under 1 sun illumination. (D) Surface of GAHAS and bulk water temperature changes with time under 1 sun illumination. (E) Evaporation rates and evaporation efficiencies of GAHAS, GAHAF, and pure water under 1 sun illumination. (F) Evaporation efficiency and evaporation rate of GAHAS under 1 sun illumination for 10 cycles.

The X-ray diffraction (XRD) curves of HGM, PHGM, AHGM, GO, and GAHAS are shown in Figure 4E; it can be seen that the curves of HGM, PHGM, AHGM, and GAHAS have broad peaks of amorphous silica at $2\theta = 15-35°$.[41] In addition, due to the reaction of HGM with NaOH, PHGM have the characteristic peaks of silicate at about $2\theta = 29°$; after grafting KH550, the transmittance of X-rays decreases, resulting in a decrease in the intensity of the characteristic peaks of the silicate on AHGM and AHGM in GAHAS.[36] Compared with GO with a characteristic diffraction peak at about $2\theta = 11°$, GAHAS has a broad peak at $2\theta = 23°$, which suggested the lower graphitized degree in GAHAS.[42]

The Raman spectra of GO and GAHAS are shown in Figure 4F. Both GO and GAHAS have two characteristic peaks corresponding to the graphite band (G-band) and defect band (D-band) at 1590 and 1350 cm^{-1}, respectively. The D-band and G-band intensity ratio (I_D/I_G) of GAHAS is higher than that of GO, resulting from the chemical reduction of GO and indicating the increase of defects.[43]

Both GAHAS and GAHAF were wetted by water droplets in a short time, and a high-speed video camera was used to record the impregnation process of one water droplet. As shown in Figure 5, two aerogels GAHAS (Figure 5A) and GAHAF (Figure 5B) were completely impregnated with water droplets within 600 ms, indicating excellent hydrophilicity, which is attributed to the hydrophilic AHGM and residual oxygen groups in RGO sheets. The hydrophilicity of the solar evaporator is beneficial to water transportation for SSG. Most importantly, both GAHAF (Figure 5C) and GAHAS (Figure 5D) can float on the water surface due to the fact that the aerogels contain hollow AHGM and ultralight RGO sheets.

The thermal stabilities of HGM, AHGM, GO, and GAHAS were measured by thermogravimetric analysis (TGA) under a N$_2$ atmosphere and the results are shown in Figure 6A. The

weight loss ratio of HGM is only 3.3% in the whole temperature range. The crystal structure of silica is extremely stable and the weight loss of HGM was mainly caused by a small amount of silanol groups on the surface of HGM.[36] Meanwhile, the weight loss ratio of AHGM was increased to 11.1% due to the weight loss of KH550 grafted on the surface. In addition, compared with GO, GAHAS exhibits better thermal stability; the weight loss is about 19% from room temperature to 200 °C and 44% when the temperature reaches 500 °C, which is mainly attributed to the release of adsorbed water and decomposition of residual oxygen-containing groups.[44]

Excellent thermal insulation is another key factor of photothermal materials for good evaporation performance. The thermal conductivity of the aerogels under both dry and wet states at room temperature is measured and the results are shown in Figure 6B. In the dry state, both GAHAS and GAHAF possess low thermal conductivity. However, the thermal conductivity of GAHAS (0.0823 W m^{-1} K^{-1}) is significantly lower than that of GAHAF (0.2317 W m^{-1} K^{-1}) in the wet state. This is because both GAHAF and GAHAS contain hollow AHGM, have porous structures, and are filled with air (about 0.026 W m^{-1} K^{-1}) in the dry state. While in the wet state, GAHAF with larger directional channels can absorb more water (about 0.59 W m^{-1} K^{-1}) than GAHAS with abundant uniform smaller pores.

A UV−vis−NIR spectrometer was used to investigate the optical absorption property of the aerogels, and the results are shown in Figure 6C. The light absorption of GAHAS (ca. 93%) is higher than that of GAHAF (ca. 85%). This is because GAHAF shines with a metal luster, while the color of GAHAS prepared by supercritical CO$_2$ drying is blacker than that of GAHAF. In addition, GAHAS with abundant pores is more conducive to light capture.
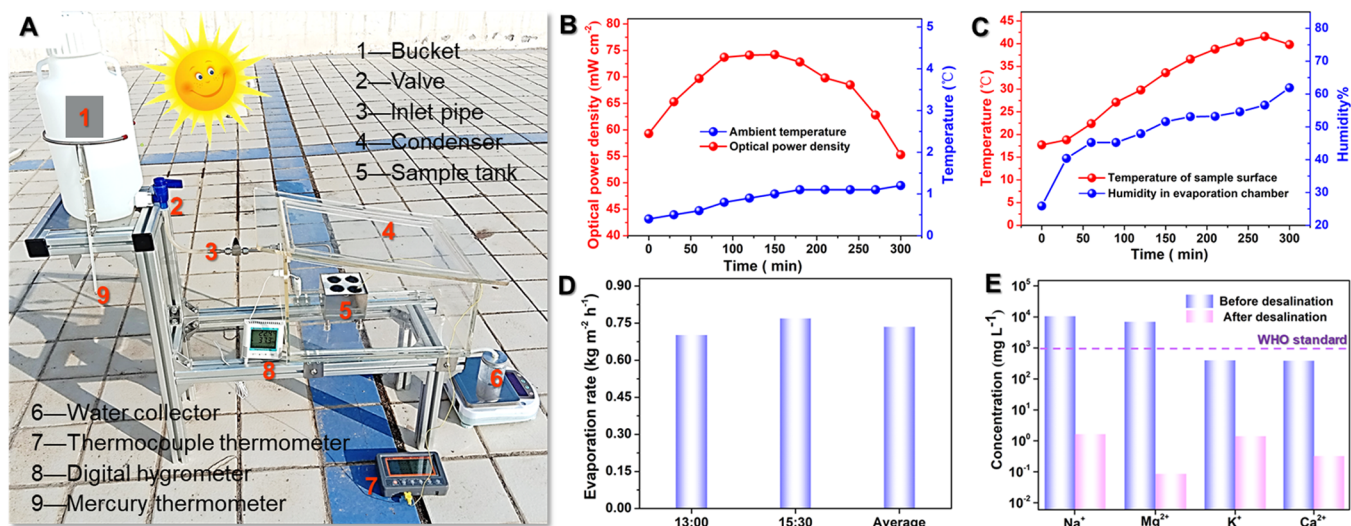
Figure 8. (A) Photograph of the outdoor desalination system for GAHAS in simulated seawater under natural sunlight. (B) Ambient temperature and optical power density change over time. (C) Temperature of the sample surface and the humidity in the desalination chamber change over time. (D) Evaporation rate of GAHAS in simulated seawater under natural sunlight. (E) Ion concentrations of the simulated seawater before and after desalination.

A good mechanical property is the guarantee for a solar evaporator to maintain long-term high-efficiency evaporation performance. As shown in Figure 6D, the aerogels containing AHGM exhibit an excellent mechanical property that could withstand a 500 g weight and without any collapse of its original structure after being removed.

3.3. SSG Performance. Benefiting from low thermal conductivity, good wettability, self-floating ability, as well as efficient solar absorption, the aerogels should be excellent photothermal materials. The SSG performances of the aerogels were evaluated by a self-made online measuring system (see details in the Supporting Information). Each test is conducted at 20−24 °C and a humidity of 15−25%. The time-dependent mass change under 1 sun illumination is shown in Figure 7A. It can be clearly seen that the water mass change of GAHAS is higher than those of GAHAF and pure water in the same evaporation time. The evaporation rate of GAHAS is 1.4856 kg m^{-2} h^{-1} under 1 sun illumination, which is higher than those of GAHAF (1.2811 kg m^{-2} h^{-1}) and pure water (0.3912 kg m^{-2} h^{-1}). In the process of the samples' evaporation performance test, the surface temperatures of GAHAS, GAHAF, and pure water were measured using an infrared camera, and the results are shown in Figure 7,CB. It can be found that the surface temperatures of aerogels and pure water increased rapidly at the beginning of light illumination and then stabilized with time under 1 sun illumination. The surface temperatures are 29.3 °C for pure water, 38.0 °C for GAHAF, and 40.2 °C for GAHAS after 30 min illumination. After 60 min, the final surface temperatures are 30.5, 39.7, and 41.4 °C, corresponding to pure water, GAHAF, and GAHAS, respectively. Obviously, the surface temperature of GAHAS is higher than those of GAHAF and pure water under the same light illumination time. The result is attributed to the fact that GAHAS exhibits better thermal insulation performance because of its lower thermal conductivity in the wet state. In order to further explain the thermal insulation performance of GAHAS, as shown in Figure 7D, below the water surface, the temperatures of T_{w1} and T_{w2} at the bulk water were measured; both T_{w1} and T_{w2} nearly had no change with time, indicating

that the heat from the surface is hardly transmitted to bulk water. The evaporation efficiency was calculated according to the reported literature studies.[45,46] For GAHAS, as shown in Figure 7E, the evaporation efficiency was calculated to be 89.13% under 1 sun illumination, which is higher than those of GAHAF (79.08%) and pure water (17.61%). All these results indicate that GAHAS exhibits better SSG performance. The main reason is, in addition to the same porous structures, the good hydrophilicity of both GAHAF and GAHAS, which can ensure fast water transmission; moreover, GAHAS has higher light absorption and a better thermal insulation property than GAHAF. In order to illustrate the SSG performance stability of the GAHAS, the SSG experiment was conducted under 1 sun illumination for 10 times and every cycle was run for 60 min. As shown in Figure 7F, the evaporation rate is relatively stable after 10 cycles, indicating the stable evaporation performance of GAHAS.

To further explore the practical desalination ability of GAHAS, the solar desalination experiment under natural sunlight was carried out in a homemade device (Figure 8A). Four pieces of GAHAS with a diameter of 3.0 cm are placed in the sample tank and covered with a square plexiglass. The simulated seawater (salinity of 3.5 wt %) was prepared according to the literature[35] and was stored in a bucket. The outdoor test was carried out from 10:30 to 15:30 for 5 h on a sunny day of November 29, 2020 in Lanzhou. As shown in Figure 8B, the ambient temperature increased from 0.4 to 1.2 °C during 10:30 to 15:30 and the optical power density increased from 59.3 to 74.2 mW cm^{-2} from 10:30 to 13:00 then decreased to 55.3 mW m^{-2} at 15:30 p.m.; the average optical power density is 67.8 mW m^{-2} (0.678 sun). Meanwhile, the temperature of the sample surface and the humidity in the desalination chamber were measured by a thermocouple thermometer and digital hygrometer, respectively. As shown in Figure 8C, the surface temperature of GAHAS was increased from 17.7 to 41.6 °C and the humidity in the desalination chamber was increased from 25.9 to 61.9%. Under these conditions, the average evaporation rate is 0.7356 kg m^{-2} h^{-1} (Figure 8D). This value is lower than that of under laboratory

measurements, which is reasonable since the outdoor experiment was conducted in winter with low ambient temperature (about 1 °C) and the average optical power density is 0.678 sun. During the 5 h desalination process, no salt was deposited on the surface of GAHAS. In addition, four major ion concentrations of Na^+, Mg^{2+}, K^+, and Ca^{2+} in simulated seawater and purified water collected at the bottom of the condenser were measured using an atomic absorption spectrometer. As shown in Figure 8E, the concentration of ions decreased sharply and the concentrations of Na^+, Mg^{2+}, K^+, and Ca^{2+} in purified water are 1.648, 0.0854, 1.42, and 0.3224 mg L^{-1}, respectively, which are far below the standard for drinking water.[47] This experiment proved that our GAHAS possessed a good solar desalination capability and showed great potential application in actual solar desalination.

4. CONCLUSIONS

In summary, we have demonstrated an approach for the first-time preparation of KH550-modified HGM-reinforced RGO composite aerogels for efficient SSG. Taking advantage of low thermal conductivity (0.0823 W m^{-1} K^{-1} in a wet state), good wettability, self-floating ability, efficient solar absorption (ca. 93%) across the full solar spectrum, as well as a porous structure with good mechanical performance, GAHAS shows an excellent energy conversion efficiency of 89.13% under 1 sun illumination and good stability. In addition, from the simulated seawater outdoor solar desalination experiment, it is found that the average evaporation rate of GAHAS is 0.7356 kg m^{-2} h^{-1} under about 0.678 natural sun illumination and that the purified water can well meet the drinking water standard. Meanwhile, the GAHAF obtained by freeze drying exhibits large directional interconnected channels and shines with a metal luster, and the thermal conductivity (0.2317 W m^{-1} K^{-1}) in a wet state is higher and light absorption (ca. 85%) is lower than GAHAS, resulting in the lower evaporation efficiency of GAHAF (79.08%) than GAHAS. Thus, the aerogel of GAHAS has great potential for practical solar desalination.

■ ASSOCIATED CONTENT

Ⓢ🅸 Supporting Information

The Supporting Information is available free of charge at https://pubs.acs.org/doi/10.1021/acsami.1c11291.

> Characterization methods; image of the hydrogels using different reagents at different hydrothermal temperatures, at different hydrothermal times, and with different concentrations of GO in the hydrothermal process; physical properties of HGM; BJH pore size distributions of GAHAF and GAHAS (PDF)

■ AUTHOR INFORMATION

Corresponding Author

An Li − *College of Petrochemical Technology, Lanzhou University of Technology, Lanzhou 730050, P. R. China;* ⓘ orcid.org/0000-0003-1982-1880; Email: lian2010@lut.cn

Authors

Shuo Wang − *College of Petrochemical Technology, Lanzhou University of Technology, Lanzhou 730050, P. R. China; Department of Chemistry and Chemical Engineering, Ankang University, Ankang, Shaanxi 725000, P. R. China*

Ye Niu − *College of Petrochemical Technology, Lanzhou University of Technology, Lanzhou 730050, P. R. China*

Chengjun Wang − *College of Petrochemical Technology, Lanzhou University of Technology, Lanzhou 730050, P. R. China*

Fei Wang − *College of Petrochemical Technology, Lanzhou University of Technology, Lanzhou 730050, P. R. China*

Zhaoqi Zhu − *College of Petrochemical Technology, Lanzhou University of Technology, Lanzhou 730050, P. R. China*

Hanxue Sun − *College of Petrochemical Technology, Lanzhou University of Technology, Lanzhou 730050, P. R. China*

Weidong Liang − *College of Petrochemical Technology, Lanzhou University of Technology, Lanzhou 730050, P. R. China*

Complete contact information is available at:
https://pubs.acs.org/10.1021/acsami.1c11291

Author Contributions

The manuscript was written through contributions of all authors. All authors have given approval to the final version of the manuscript.

Notes

The authors declare no competing financial interest.

■ ACKNOWLEDGMENTS

■ REFERENCES

(1) Veldkamp, T. I. E.; Wada, Y.; Aerts, J. C. J. H.; Döll, P.; Gosling, S. N.; Liu, J.; Masaki, Y.; Oki, T.; Ostberg, S.; Pokhrel, Y.; Satoh, Y.; Kim, H.; Ward, P. J. Water Scarcity Hotspots Travel Downstream due to Human Interventions in the 20th and 21st Century. *Nat. Commun.* **2017**, *8*, 15697.

(2) Greve, P.; Kahil, T.; Mochizuki, J.; Schinko, T.; Satoh, Y.; Burek, P.; Fischer, G.; Tramberend, S.; Burtscher, R.; Langan, S.; Wada, Y. Global Assessment of Water Challenges under Uncertainty in Water Scarcity Projections. *Nat. Sustain.* **2018**, *1*, 486−494.

(3) Lv, H.; Wang, Y.; Wu, L.; Hu, Y. Numerical Simulation and Optimization of the Flash Chamber for Multi-stage Flash Seawater Desalination. *Desalination* **2019**, *465*, 69−78.

(4) Baccioli, A.; Antonelli, M.; Desideri, U.; Grossi, A. Thermodynamic and Economic Analysis of the Integration of Organic Rankine Cycle and Multi-Effect Distillation in Waste-heat Recovery Applications. *Energy* **2018**, *161*, 456−469.

(5) Verbeke, R.; Gómez, V.; Vankelecom, I. F. J. Chlorine-resistance of Reverse Osmosis (RO) Polyamide Membranes. *Prog. Polym. Sci.* **2017**, *72*, 1−15.

(6) Ebrahimi, A.; Saharkhiz, M. H. M.; Ghorbani, B. Thermodynamic Investigation of a Novel Hydrogen Liquefaction Process Using Thermo-electrochemical Water Splitting Cycle and Solar Collectors. *Energy Convers. Manage.* **2021**, *242*, 114318.

(7) Fagiolari, L.; Bonomo, M.; Cognetti, A.; Meligrana, G.; Gerbaldi, C.; Barolo, C.; Bella, F. Photoanodes for Aqueous Solar Cells: Exploring Additives and Formulations Starting from a Commercial TiO_2 Paste. *ChemSusChem* **2020**, *13*, 6562−6573.

(8) Abdel-Wahed, M. S.; El-Kalliny, A. S.; Badawy, M. I.; Attia, M. S.; Gad-Allah, T. A. Core Double-shell $MnFe_2O_4$@rGO@TiO_2 Superparamagnetic Photocatalyst for Wastewater Treatment under Solar Light. *Chem. Eng. J.* **2020**, *382*, 122936.

(9) Liu, X.; Cheng, P.; Zhang, X.; Shen, T.; Liu, J.; Ren, J.-C.; Wang, H.; Li, S.; Liu, W. Enhanced Solar-to-hydrogen Efficiency for Photocatalytic Water Splitting Based on a Polarized Heterostructure:

the Role of Intrinsic Dipoles in Heterostructures. *J. Mater. Chem. A* **2021**, *9*, 14515−14523.

(10) Xu, W.; Xing, Y.; Liu, J.; Wu, H.; Cui, Y.; Li, D.; Guo, D.; Li, C.; Liu, A.; Bai, H. Efficient Water Transport and Solar Steam Generation via Radially, Hierarchically Structured Aerogels. *ACS Nano* **2019**, *13*, 7930−7938.

(11) Lu, Q.; Shi, W.; Yang, H.; Wang, X. Nanoconfined Water-Molecule Channels for High-Yield Solar Vapor Generation under Weaker Sunlight. *Adv. Mater.* **2020**, *32*, 2001544.

(12) Irshad, M. S.; Wang, X.; Abbasi, M. S.; Arshad, N.; Chen, Z.; Guo, Z.; Yu, L.; Qian, J.; You, J.; Mei, T. Semiconductive, Flexible MnO_2 NWs/Chitosan Hydrogels for Efficient Solar Steam Generation. *ACS Sustainable Chem. Eng.* **2021**, *9*, 3887−3900.

(13) Wang, S.; Fan, Y.; Wang, F.; Su, Y.; Zhou, X.; Zhu, Z.; Sun, H.; Liang, W.; Li, A. Potentially Scalable Fabrication of Salt-rejection Evaporator Based on Electrogenerated Polypyrrole-coated Nickel Foam for Efficient Solar Steam Generation. *Desalination* **2021**, *505*, 114982.

(14) He, J.; Zhang, Z.; Xiao, C.; Liu, F.; Sun, H.; Zhu, Z.; Liang, W.; Li, A. High-Performance Salt-Rejecting and Cost-Effective Super-hydrophilic Porous Monolithic Polymer Foam for Solar Steam Generation. *ACS Appl. Mater. Interfaces* **2020**, *12*, 16308−16318.

(15) Qin, Z.; Sun, H.; Tang, Y.; Yin, S.; Yang, L.; Xu, M.; Liu, Z. Bioinspired Hydrophilic−Hydrophobic Janus Composites for Highly Efficient Solar Steam Generation. *ACS Appl. Mater. Interfaces* **2021**, 19467.

(16) Li, K.; Gao, M.; Li, Z.; Yang, H.; Jing, L.; Tian, X.; Li, Y.; Li, S.; Li, H.; Wang, Q.; Ho, J. S.; Ho, G. W.; Chen, P.-Y. Multi-interface Engineering of Solar Evaporation Devices via Scalable, Synchronous Thermal Shrinkage and Foaming. *Nano Energy* **2020**, *74*, 104875.

(17) Guo, A.; Fu, Y.; Wang, G.; Wang, X. Diameter Effect of Gold Nanoparticles on Photothermal Conversion for Solar Steam Generation. *RSC Adv.* **2017**, *7*, 4815−4824.

(18) Wang, F.; Hu, Z.; Fan, Y.; Bai, W.; Wu, S.; Sun, H.; Zhu, Z.; Liang, W.; Li, A. Salt-Rejection Solar Absorbers Based on Porous Ionic Polymers Nanowires for Desalination. *Macromol. Rapid Commun.* **2021**, *42*, 2000536.

(19) Shao, Y.; Jiang, Z.; Zhang, Y.; Wang, T.; Zhao, P.; Zhang, Z.; Yuan, J.; Wang, H. All-Poly(ionic liquid) Membrane-Derived Porous Carbon Membranes: Scalable Synthesis and Application for Photothermal Conversion in Seawater Desalination. *ACS Nano* **2018**, *12*, 11704−11710.

(20) Storer, D. P.; Phelps, J. L.; Wu, X.; Owens, G.; Khan, N. I.; Xu, H. Graphene and Rice-Straw-Fiber-Based 3D Photothermal Aerogels for Highly Efficient Solar Evaporation. *ACS Appl. Mater. Interfaces* **2020**, *12*, 15279−15287.

(21) Wang, C.; Wang, J.; Li, Z.; Xu, K.; Lei, T.; Wang, W. Superhydrophilic Porous Carbon Foam as a Self-desalting Monolithic Solar Steam Generation Device with High Energy Efficiency. *J. Mater. Chem. A* **2020**, *8*, 9528−9535.

(22) Yang, L.; Chen, G.; Zhang, N.; Xu, Y.; Xu, X. Sustainable Biochar-Based Solar Absorbers for High-Performance Solar-Driven Steam Generation and Water Purification. *ACS Sustainable Chem. Eng.* **2019**, *7*, 19311−19320.

(23) He, J.; Fan, Y.; Xiao, C.; Liu, F.; Sun, H.; Zhu, Z.; Liang, W.; Li, A. Enhanced Solar Steam Generation of Hydrogel Composite with Aligned Channel and Shape Memory Behavior. *Compos. Sci. Technol.* **2021**, *204*, 108633.

(24) Sun, Y.; Gao, J.; Liu, Y.; Kang, H.; Xie, M.; Wu, F.; Qiu, H. Copper Sulfide-Macroporous Polyacrylamide Hydrogel for Solar Steam Generation. *Chem. Eng. Sci.* **2019**, *207*, 516−526.

(25) Yin, X.; Zhang, Y.; Guo, Q.; Cai, X.; Xiao, J.; Ding, Z.; Yang, J. Macroporous Double-Network Hydrogel for High-Efficiency Solar Steam Generation Under 1 sun Illumination. *ACS Appl. Mater. Interfaces* **2018**, *10*, 10998−11007.

(26) Ding, T.; Zhou, Y.; Ong, W. L.; Ho, G. W. Hybrid Solar-Driven Interfacial Evaporation Systems: Beyond Water Production Towards High Solar Energy Utilization. *Mater. Today* **2021**, *42*, 178−191.

(27) Yang, M. Q.; Tan, C. F.; Lu, W.; Zeng, K.; Ho, G. W. Spectrum Tailored Defective 2D Semiconductor Nanosheets Aerogel for Full-Spectrum-Driven Photothermal Water Evaporation and Photochemical Degradation. *Adv. Funct. Mater.* **2020**, *30*, 2004460.

(28) Mu, P.; Zhang, Z.; Bai, W.; He, J.; Sun, H.; Zhu, Z.; Liang, W.; Li, A. Superwetting Monolithic Hollow-Carbon-Nanotubes Aerogels with Hierarchically Nanoporous Structure for Efficient Solar Steam Generation. *Adv. Energy Mater.* **2019**, *9*, 1802158.

(29) Mei, T.; Chen, J.; Zhao, Q.; Wang, D. Nanofibrous Aerogels with Vertically Aligned Microchannels for Efficient Solar Steam Generation. *ACS Appl. Mater. Interfaces* **2020**, *12*, 42686−42695.

(30) Wang, Y.; Wu, X.; Gao, T.; Lu, Y.; Yang, X.; Chen, G. Y.; Owens, G.; Xu, H. Same Materials, Bigger Output: A Reversibly Transformable 2D−3D Photothermal Evaporator for Highly Efficient Solar Steam Generation. *Nano Energy* **2021**, *79*, 105477.

(31) Geng, H.; Liu, J.; Guo, A.; Ren, S.; Xu, X.; Liu, S. Fabrication of Heat-Resistant Syntactic Foams Through Binding Hollow Glass Microspheres with Phosphate Adhesive. *Mater. Des.* **2016**, *95*, 32−38.

(32) Xu, R.; Wang, W.; Yu, D. Preparation of Silver-Plated Hollow Glass Microspheres and its Application in Infrared Stealth Coating Fabrics. *Prog. Org. Coat.* **2019**, *131*, 1−10.

(33) Zhang, Y.-l.; Zang, C.-g.; Jiao, Q.-j.; She-li, Y.-f. Heat-Insulating Materials with High-Temperature Resistance Through Binding Hollow Glass Microspheres with Vinyl-Functionalized Polyborosiloxane. *J. Mater. Sci.* **2020**, *55*, 14264−14279.

(34) Long, J.; Jiang, C.; Zhu, J.; Song, Q.; Hu, J. Controlled TiO_2 Coating on Hollow Glass Microspheres and Their Reflective Thermal Insulation Properties. *Particuology* **2020**, *49*, 33−39.

(35) Wang, F.; Mu, P.; Zhang, Z.; Chen, T.; Li, Y.; Sun, H.; Zhu, Z.; Liang, W.; Li, A. Reduced Graphene Oxide Coated Hollow Polyester Fibers for Efficient Solar Steam Generation. *Energy Technol.* **2019**, *7*, 1900265.

(36) An, Y.; Zheng, H.; Zheng, X.; Sun, Q.; Zhou, Y. Use of a Floating Adsorbent to Remove Dyes from Water: A Novel Efficient Surface Separation Method. *J. Hazard. Mater.* **2019**, *375*, 138−148.

(37) Park, B.-D.; Wi, S. G.; Lee, K. H.; Singh, A. P.; Yoon, T.-H.; Kim, Y. S. X-ray Photoelectron Spectroscopy of Rice Husk Surface Modified with Maleated Polypropylene and Silane. *Biomass Bioenergy* **2004**, *27*, 353−363.

(38) Thommes, M.; Kaneko, K.; Neimark, A. V.; Olivier, J. P.; Rodriguez-Reinoso, F.; Rouquerol, J.; Sing, K. S. W. Physisorption of Gases, with Special Reference to the Evaluation of Surface Area and Pore Size Distribution (IUPAC Technical Report). *Pure Appl. Chem.* **2015**, *87*, 1051−1069.

(39) Xu, X.; Zhang, Q.; Yu, Y.; Chen, W.; Hu, H.; Li, H. Naturally Dried Graphene Aerogels with Superelasticity and Tunable Poisson's Ratio. *Adv. Mater.* **2016**, *28*, 9223−9230.

(40) Hu, H.; Zhao, Z.; Wan, W.; Gogotsi, Y.; Qiu, J. Ultralight and Highly Compressible Graphene Aerogels. *Adv. Mater.* **2013**, *25*, 2219−2223.

(41) Yao, Q.; Shi, W.; Feng, G.; Lu, Z.-H.; Zhang, X.; Tao, D.; Kong, D.; Chen, X. Ultrafine Ru Nanoparticles Embedded in SiO_2 Nanospheres: Highly Efficient Catalysts for Hydrolytic Dehydrogenation of Ammonia Borane. *J. Power Sources* **2014**, *257*, 293−299.

(42) Sun, H.; Li, Y.; Zhu, Z.; Mu, P.; Wang, F.; Liang, W.; Ma, C.; Li, A. Photothermal Conversion Material Derived from Used Cigarette Filters for Solar Steam Generation. *ChemSusChem* **2019**, *12*, 4257−4264.

(43) Jiang, Y.; Xu, Z.; Huang, T.; Liu, Y.; Guo, F.; Xi, J.; Gao, W.; Gao, C. Direct 3D Printing of Ultralight Graphene Oxide Aerogel Microlattices. *Adv. Funct. Mater.* **2018**, *28*, 1707024.

(44) Du, Y.; Dong, N.; Zhang, M.; Zhu, K.; Na, R.; Zhang, S.; Sun, N.; Wang, G.; Wang, J. Covalent Functionalization of Graphene Oxide with Porphyrin and Porphyrin Incorporated Polymers for Optical Limiting. *Phys. Chem. Chem. Phys.* **2017**, *19*, 2252−2260.

(45) Hong, S.; Shi, Y.; Li, R.; Zhang, C.; Jin, Y.; Wang, P. Nature-Inspired, 3D Origami Solar Steam Generator toward Near Full Utilization of Solar Energy. *ACS Appl. Mater. Interfaces* **2018**, *10*, 28517−28524.

(46) Yang, J.; Pang, Y.; Huang, W.; Shaw, S. K.; Schiffbauer, J.; Pillers, M. A.; Mu, X.; Luo, S.; Zhang, T.; Huang, Y.; Li, G.; Ptasinska, S.; Lieberman, M.; Luo, T. Functionalized Graphene Enables Highly Efficient Solar Thermal Steam Generation. *ACS Nano* **2017**, *11*, 5510−5518.

(47) Smith, A. H.; Lopipero, P. A.; Bates, M. N.; Steinmaus, C. M. Arsenic Epidemiology and Drinking Water Standards. *Science* **2002**, *296*, 2145−2146.